Cement and Concrete Research 39 (2009) 1077–1086

Contents lists available at ScienceDirect

Cement and Concrete Research

journal homepage: http://ees.elsevier.com/CEMCON/default.asp

The corrosion pattern of reinforcement and its influence on serviceability of reinforced concrete members in chloride environment

Ruijin Zhang [a,*], Arnaud Castel [b], Raoul François [b]

[a] Northeastern University, Shenyang, China
[b] Université de Toulouse, UPS, INSA, LMDC, Laboratoire Matériaux et Durabilité des Constructions, 137 Avenue de Rangueil, F 31077 Toulouse, France

ARTICLE INFO

Article history:
Received 9 April 2008
Accepted 26 July 2009

Keywords:
Crack Detection (B)
Corrosion (C)
Long-Term Performance (C)
Bond Strength (C)
Reinforcement (D)

ABSTRACT

This paper deals with two corroded reinforcement concrete beams, which have been stored under sustained load in a chloride environment for 14 and 23 years respectively. The evolution of corrosion pattern of reinforcement and its influence on serviceability are studied. In chloride-induced corrosion process, corrosion cracking affects significantly the corrosion pattern. During the corrosion cracking initiation period, only local pitting corrosion occurs. At early stage of cracking propagation, localized pitting corrosion is still predominant as cracks widths are very small and cracks are not interconnected, but a general corrosion slowly develops as the cracks widen. At late cracking stage, interconnected cracking with wide width develops along large parts of the beam leading to a general corrosion pattern. Macrocells and microcells concepts are used for the interpretation of the results.

Mechanical experiments and corrosion simulation tests are performed to clarify the influence of this corrosion pattern evolution on the serviceability of the beams (deflection increase). Experimental results show that, when the corrosion is localized (early cracking stage), the steel–concrete bond loss is the main factor affecting the beams serviceability. The local cross-section loss resulting from pitting attack does not significantly influence the deflection of the beam. When corrosion is generalized (late cracking stage), as the steel–concrete bond is already lost, the generalized steel cross-section reduction becomes the main factor affecting the beams serviceability. But, at this stage, the deflection increase is slower due to the low general corrosion rate.

© 2009 Elsevier Ltd. All rights reserved.

1. Introduction

The deterioration of reinforced concrete structures due to chloride-induced corrosion is a major problem all over the world. Reinforcement corrosion affects the safety and the serviceability of concrete structures by increasing deflection, reducing the bearing capacity and the ductility [1–4]. The longitudinal corrosion cracking leads to a reduction of the steel–concrete bond strength [5,6]. Between two flexural cracks, as a part of the tensile load is transferred from the steel to the concrete thanks to the bond (tension stiffening effect), the steel–concrete bond loss is considered as one of the major factor influencing the serviceability (beam deflection).

Few literatures dealing with the evolution of steel corrosion pattern in a long term natural corrosion process are available. In this paper, experiments are carried out on two corroded RC-beam and one control beam. The two corroded beams were exposed to a chloride environment for 14 or 23 years under sustained load. The corrosion cracking maps of the corroded beams were drawn and mechanical tests under service loading were performed at different periods. Then, tests up to failure were carried out. After the failure, the distribution of the corrosion along the reinforcing bars was accurately assessed. Correlation between corrosion pattern evolution and beams deflection increase was studied. Moreover, experimental simulations of corrosion were performed on a control beam for a better understanding of the respective effects of the bond loss, the local or general steel cross-section reduction on the serviceability.

2. Experimental context

This work is based on a long term experimental program started in 1984 at the Laboratoire Matériaux et Durabilité des Constructions (L.M.D.C.) in Toulouse (France). 36 RC-beams with two different sections (types A and B) were cast and stored in a chloride environment under sustained loading. Beams A were cast with 40 mm concrete cover and beams B with 10 mm concrete cover (corresponding to the maximum and minimum cover according to French standards at the time of manufacturing). At different periods, tests were carried out to collect experimental data such as cracking maps, chloride content, and mechanical behaviour under service loading. Some of them have been tested up to failure in order to

* Corresponding author. Modern design and analysis research institute, Northeastern University, Shenyang, 110003, China.
E-mail address: rjzhang@mail.neu.edu.cn (R. Zhang).

0008-8846/$ – see front matter © 2009 Elsevier Ltd. All rights reserved.
doi:10.1016/j.cemconres.2009.07.025

assess the ultimate capacity and the real corrosion distribution along the reinforcing bars. In this paper, only the experimental results obtained on two corroded type B beams after 14 and 23 years are reported.

2.1. Reinforced concrete specimens

The layout of the reinforcement of the RC-beam B is shown in Fig. 1. The concrete and the cement compositions are given in Table 1 and Table 2. Water content was adjusted to obtain a slump of 70 mm. After 28 days, the average compressive strength and the elastic modulus obtained on cylinder specimens (110×220 mm) were 45 MPa and 32 GPa respectively.

2.2. Conservation modes

All the beams were loaded in 3-point bending. Two loading values were used: $M_{ser1} = 13.5$ kN m (beams labelled B1CL) or $M_{ser2} = 21.2$ kN m (beams labelled B2CL). M_{ser1} corresponds to about 50% of the failure load; the maximum stress in the tensile steel σ_s was 240 MPa (Ultimate limit state design in non-aggressive environment according to French standards). M_{ser2} corresponds to about 80% of the failure load; the maximum stress in the tensile steel σ_s was 380 MPa (about two times the Serviceability limit state design in chloride environment according to French standards).

The aggressive environment was a salt fog (35 g/l of NaCL corresponding to the chloride concentration of sea water). The beams have been stored under loading in a confined room with four sprays located at each upper corner. The conservation mode of the beams was:

- 0 to 6 years: cycles of 15 drying days and 7 wetting days under laboratory conditions ($T \approx 20$ °C),
- 6 to 9 years: cycles of 7 drying days and 7 wetting days under laboratory conditions ($T \approx 20$ °C),
- 9 to 19 years: cycles of 7 drying days and 7 wetting days, however the confined room was transferred outside, so the beams were exposed to the temperature of the southwest of France,
- 19 to 23 years: cycles have been stopped and the beams were unloaded and stored in the confined room and exposed to the temperature of the southwest of France.

In comparison with in-site structures at the seashore, the high loading level and the regular wetting/drying cycles imposed to the beams lead to an accelerated version of the real corrosion process. The low concrete cover (10 mm) of type B beams also contributes to accelerate the corrosion deteriorations. However, concerning the corrosion distribution and the composition of the oxides produced, the process is much closer to that observed in natural conditions than when an electrical potential is applied in order to accelerate the corrosion [7,8].

Type B control beams were also available, stored in the laboratory environment with a constant temperature ($T \approx 20$ °C) and subjected to wetting cycles during the first six years. During the first seventeen years, they were loaded in 3-point bending like the corroded beams.

Table 1
Concrete composition (kg/m^3).

Mix component		
Rolled gravel (silica + limestone)	5/15 mm	1220
Sand	0/5 mm	820
Portland cement: OPC HP (high perform)		400
Water		200

3. Experimental program

The two beams used in this paper are labelled B1CL1 and B2CL1. B1CL1 was tested up to failure after 14 years and B2CL1 after 23 years. A control beam labelled BT is used to perform the experimental simulation of corrosion.

3.1. Cracking maps

At first, the cracking maps of beams B1CL1 and B2CL1 were drawn with the exact locations of the transversal cracks and the longitudinal corrosion cracks after 14, 19 and 23 years. Only the longitudinal crack widths were indicated, which were measured using a binocular lens with an accuracy of 0.02 mm.

3.2. Assessment of the reinforcement cross-section loss

The corrosion distribution along the reinforcements of B1CL1 and B2CL1 was measured after the failure tests. The steel cross-section reduction was assessed from the mass loss after the covering concrete was completely removed. Reference mass per unit of length m was determined using non-corroded part of the rebar. In corroded areas, the residual mass per unit of length was measured after cleaning the corrosion products (using Clark's solution ANSI/ASTM G1-72) and then related to the reference mass. The average reinforcement mass loss per unit of length Δm was then calculated. In the case of local pitting attacks, the length of the samples could be less than 5 mm. The steel cross-section loss ΔA_s was finally deduced from the loss of mass Δm using the following equation:

$$\Delta A_s = \frac{\Delta m}{m} \cdot A_s$$

Where ΔA_s is the average steel cross-section loss (mm^2) on the sampling length, A_s is the sound steel cross-section (mm^2) and m is the reference mass per unit of length. A more detailed physico-chemical study of beam B1CL1 is already available [9].

3.3. Serviceability of the corroded and control beams

Only the evolution of serviceability was analysed by measuring the mid-span deflection under a constant rate loading in three-point flexion up to 13.5 kN m. The service loading ($M_{ser} = 13.5$ kN m) corresponds to a

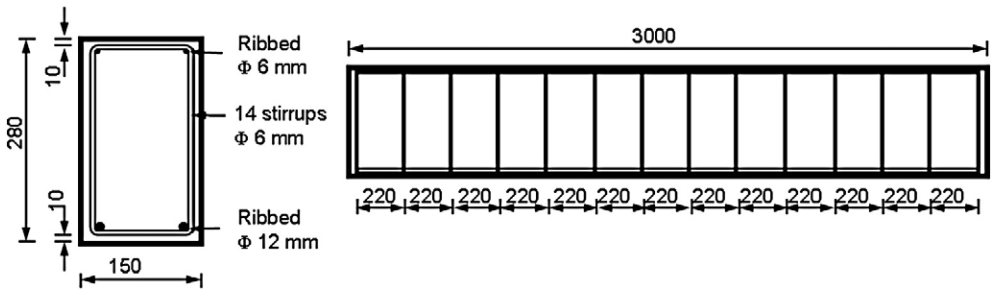

Fig. 1. The layout of the type B beams reinforcement (all dimension in mm).

Table 2
Cement chemical composition (%).

	SiO_2	Al_2O_3	Fe_2O_3	CaO	MgO	SO_3	Na_2O
Weight	21.4	6.0	2.3	63.0	1.4	3.0	0.5

force of 20 kN at the mid-span. The vertical displacement was measured using a digital displacement sensor with an accuracy of 0.01 mm.

3.4. Experimental simulation of corrosion

The process of steel–concrete bond degradation is complex and depends on the corrosion state of the steel bars. It was not possible to simulate a partial degradation of the bond, only a total bond loss is considered during the corrosion simulations. These simulations represent an extreme corrosion situation regarding bond. The pitting attack is characteristic of natural chloride corrosion, then, several local cross-section reductions were simulated on the control beam BT to clarify their influence on the serviceability.

The service load was $M_{ser1} = 13.5$ kN m (i.e. 20 kN loading). The total loss of bond strength was simulated by removing the concrete cover around the steel. The local cross-section reduction was simulated by sawing local notches on the reinforcing bars. First of all, beam BT was divided into several sectors of about 200 mm length (Fig. 2). This length corresponds to the stirrups and the bending cracks spacing because the flexural cracks always occur in front of the stirrups. Previous works [9,10] showed that the corrosion is mostly located in the central part of the tensile re-bars (highest bending moment area). So, the simulation of the bond loss was performed in the central part of beam, and the simulation of steel cross-section loss due to pitting attack was only performed in the maximum moment area (zone E, Fig. 2). The simulation tests are performed as followed:

- The initial behaviour of the control beam was measured (noted as BT);
- The concrete cover around the front tensile rebar was removed in the central sector E (noted as BTE1);
- The concrete cover around another tensile rebar was removed in sector E, which resulted in a total loss of bond in this zone (noted as BTE2);
- A notch ES1 was performed on the front tensile rebar at the midpoint of sector E. Its depth was about 3 mm corresponding to 20% cross-section reduction (noted as BTES1, Fig. 3(a));
- One notch ES2 was performed on the back rebar in sector E but not at the midpoint (Fig. 3(b)). Its depth was also about 3 mm (noted as BTES2);
- The second notch ES3 on the back rebar was performed in sector E but still not at midpoint (Fig. 3(b)). Its depth was about 3.5 mm corresponding to a 25% cross-section reduction (noted as BTES3);
- The third notch ES4 on the back rebar was performed at the midpoint of sector E then in front of the notch ES1. Its depth was about 4 mm corresponding to 30% cross-section reduction (noted as BTES4, Fig. 3(b));
- Both sides of concrete cover were removed in sector F (noted as BTF2);
- Both sides of concrete cover were removed in sector D (noted as BTD2).

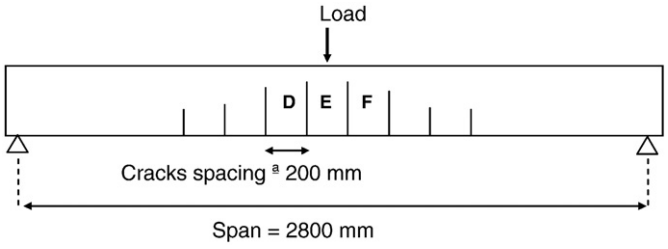

Fig. 2. Identification of the sectors of beam BT for the corrosion simulation.

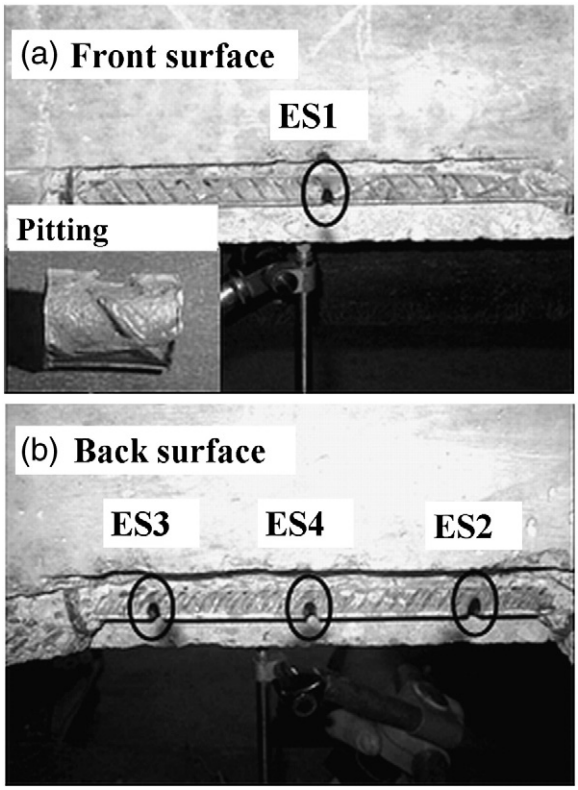

Fig. 3. Notches performed on the tensile re-bars of beam BT in sector E after the removing of concrete cover.

4. Experimental results

4.1. Cracking maps

Figs. 4 to 7 show the cracking maps of B2CL1 and B2CL1 after 14, 19 and 23 years of exposure respectively. Only the cracking map after 14 years is available for B1CL1.

After 14 years (Figs. 4 and 5), many small and independent longitudinal cracks were observed along the tensile re-bars of both beams. Almost all cracks were less than 0.5 mm width and located in the central zone. The cracks along the compressive re-bars were always randomly distributed along the beams. For beam B1CL1 (Fig. 4), only one crack located at mid-span of the back surface reached 1.4 mm width. The maximum crack width observed along the tensile re-bars of beam B2CL1 (Fig. 5) reached 2 mm width, but was not located at mid-span. The cracks distributions along B1CL1 and B2CL1 after 14 years were quite different.

For B2CL1 after 19 years and 23 years of exposure, corrosion cracking developed along both tensile and compressive re-bars (Figs. 6 and 7). The map after 23 years shows wider and longer longitudinal cracks in comparison with the one after 19 years. In Fig. 7, the cracks along the tensile re-bars are interconnected and extended along the beam. 3 mm maximum crack width is observed at mid-span in the tension zone. In the compressive zone, the cracks are still randomly distributed along the re-bars. The maximum crack width reaches 1 mm and 2.8 mm after 19 and 23 years respectively.

4.2. Observation of corrosion pattern

Along the re-bars sampled on the beams B1CL1 and B2CL1, red and brownish-red coloured rusts were observed in different amounts and at different locations. The re-bars of beam B2CL1 after 23 years of exposure were a lot more corroded than the ones of beam B1CL1 after

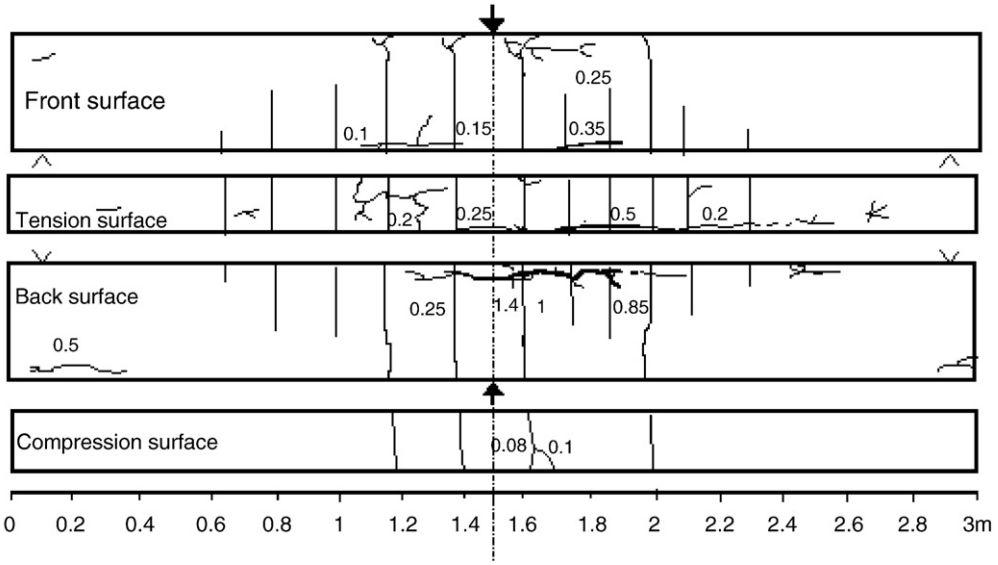

Fig. 4. Cracking maps of B1CL1 after 14 years of exposure (crack widths in mm).

only 14 years and the central parts of the tensile rebar were always the most corroded.

For B1CL1, pitting attacks were always observed at the vicinity of all corrosion cracks along the tensile bars (Fig. 8(b)), except a slight general corrosion observed along the widest corrosion crack in the central zone (Fig. 8(a)). The localized pitting corrosion was the predominant corrosion pattern for the tension re-bars of beam B1CL1. On the contrary, for the tensile re-bars of B2CL1, corrosion has extended all along the beam, in accordance with the wide and long longitudinal cracks observed in the tensile zone (Fig. 7). Several pitting attacks were observed; but the corrosion was generalized all along the re-bars. Generalized corrosion became the predominant corrosion pattern (Fig. 9).

For the compressive re-bars of both beams, a general corrosion occurred on the lower half surface of the steel according to the concrete casting direction, where voids were formed due to the effect of bleeding ("top-bar" effect). Some severe pitting attacks were also observed at the location of the main corrosion cracks. The corrosion propagation related to the "top-bar" effect will be discussed further.

4.3. Distribution of reinforcement cross-section loss

Figs. 10 to 13 show the real distribution of the cross-section loss for all re-bars, measured on B1CL1 and B2CL1 after 14 years and 23 years respectively.

Fig. 10 shows that the corrosion of the tensile re-bars of B1CL1 was more concentrated in the central part where the bending moment is the highest and the corrosion cracks were the widest. The maximum average (on two bars) cross-section reduction was about 19% at the mid-span.

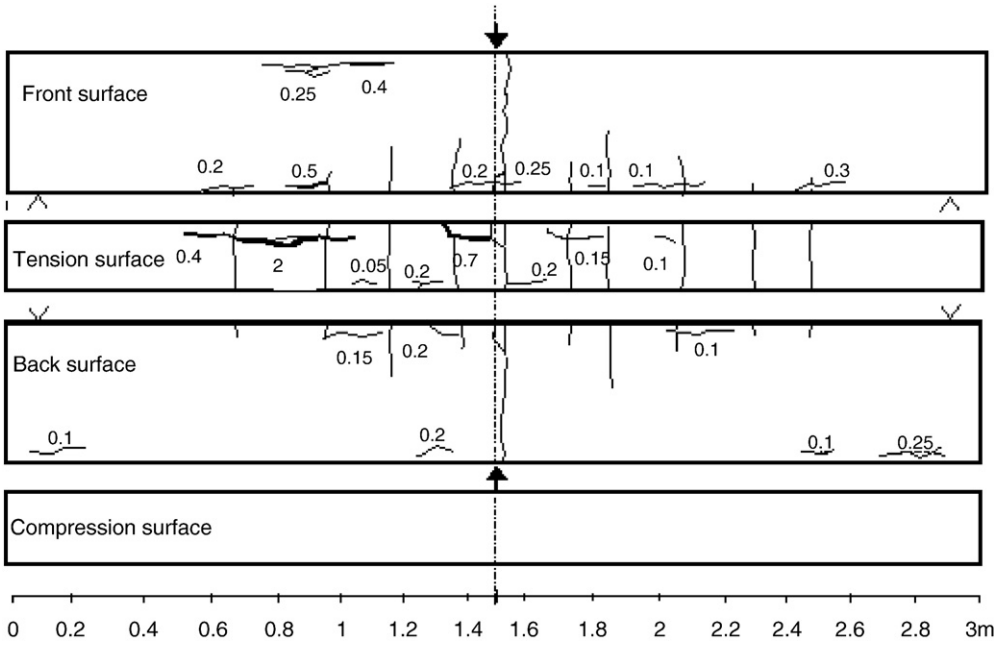

Fig. 5. Cracking maps of B2CL1 after 14 years of exposure (crack widths in mm).

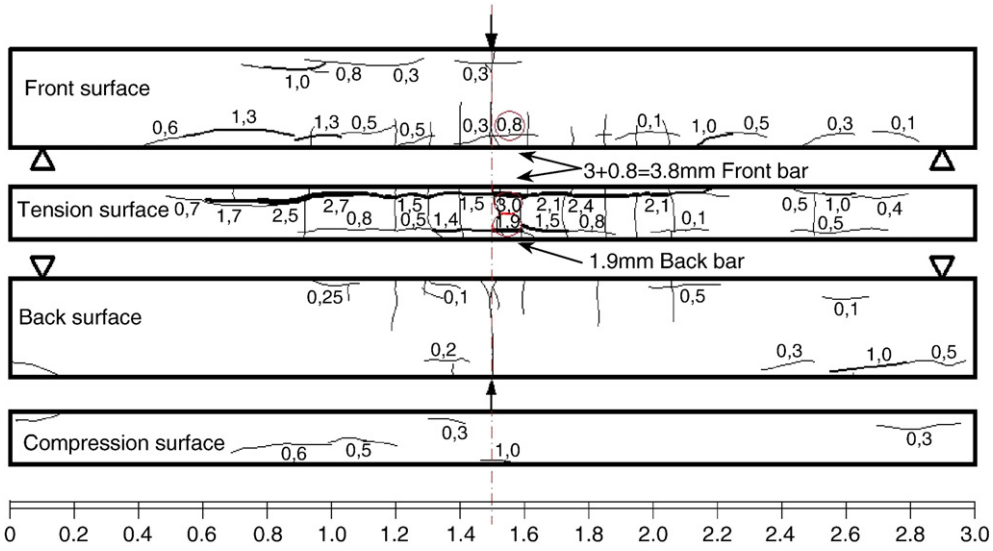

Fig. 6. Cracking maps of B2CL1 after 19 years of exposure (crack widths in mm).

For the compressive re-bars (Fig. 11), as for the corrosion cracks, the corrosion is randomly distributed along the beam. The maximum cross-section loss (18 mm^2) for the back re-bar occurred near the support, corresponding to the location of the 0.5 mm crack width.

B2CL1 tensile re-bars were more corroded than B1CL1 ones, as show in Fig. 12. On the front tensile rebar, the maximum local cross-section loss was about 46 mm^2 (40% cross-section reduction) and was located at about 200 mm on the left of the mid-span. The maximum cross-section loss due to the generalized corrosion reaches 40 mm^2, and was located along the front reinforcement in correspondence to the 4.2 mm crack width location. The corrosion of B2CL1 compressive bars (Fig. 13) was similar to the one observed on B1CL1.

4.4. Mechanical experiments—corrosion simulations

Fig. 14 presents the mid-span deflections measured for the 9 steps of the corrosion simulation performed on BT control beam under service loading (13.5 kN m). B1CL1 deflection after 14 years and B2CL1 deflections after 14, 19 and 23 years are also presented in Fig. 14. The results show that the steel–concrete bond strength deterioration had a significant effect on the stiffness of the beam. In zone E (Fig. 2), the removal of concrete cover around a single tensile reinforcement (BTE1) resulted in a 15% increase of the deflection, and the loss of bond on both sides (BTE2) resulted in a 31% total increase. However, for the section losses of up to 25% used in this study, the local steel cross-section reduction had no significant influence on the global stiffness of the beam. Indeed, the deflection rises from 1.99 mm to 2.09 mm (about 5%), which is not significant according to the scatters of the measure (around 0.05 mm). Finally, the total bond loss in zone E (BTE2), F (BTEF2) and D (BTED2) induced a deflection increase of respectively 0.47 mm, 0.38 mm and 0.34 mm. It was obvious that a bond loss in the central zone (E) had more influence on the global behaviour because it was the area of the maximum bending moment. Therefore, the propagation of the bond loss along the span (D and F) has contributed significantly to the global reduction of the bending stiffness.

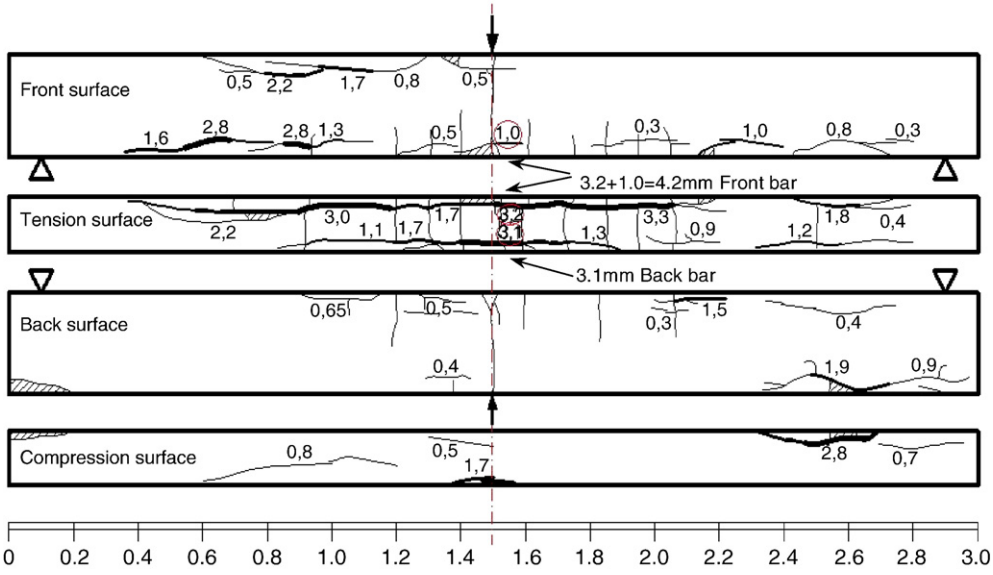

Fig. 7. Cracking maps of B2CL1 after 23 years of exposure (crack widths in mm, and the hatched parts represent concrete that has fallen off).

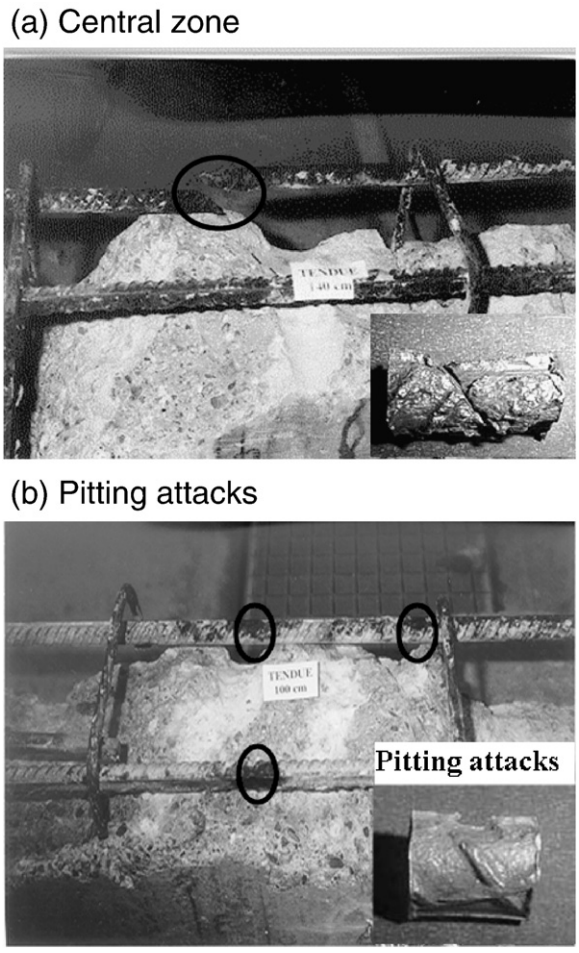

Fig. 8. Corrosion on the tensile steel bars of B1CL1 after 14 years.

For the 14 years old corroded beams, due to the higher corrosion crack width (1.4 mm) located at mid-span, the maximum deflection, measured on B1CL1, has increased more than 50% compared to the control beam. After 14 years, the deflection increase observed on B2CL1 was a lot lower. Indeed, the corrosion cracking along the tensile bars of B2CL1 was located far from the maximum moment zone and did not affect significantly the deflection.

After a 19 years period, the B2CL1 deflection has also increased significantly. This important reduction of stiffness was due to the high propagation (between 14 and 19 years) of corrosion cracking at mid-span along both tensile reinforcing bars with several corrosion cracks reaching 3 mm width.

After a period of 23 years, the deflection measured on B2CL1 was almost equivalent to the one measured after 19 years, even if the corrosion cracking in the tension area was more developed than that after 19 years. For B2CL1, cumulated cracks width on the four surfaces of the beam at mid-span propagated from 5.7 mm (0.8 + 3 + 1.9 mm) after 19 years to 7.3 mm (1 + 3.2 + 3.1) after 23 years (Figs. 6 and 7). This important increase of corrosion cracks width has resulted obviously from an important increase of steel reinforcing bars corrosion. But the increase in deflection between 17 years and 23 years was very low.

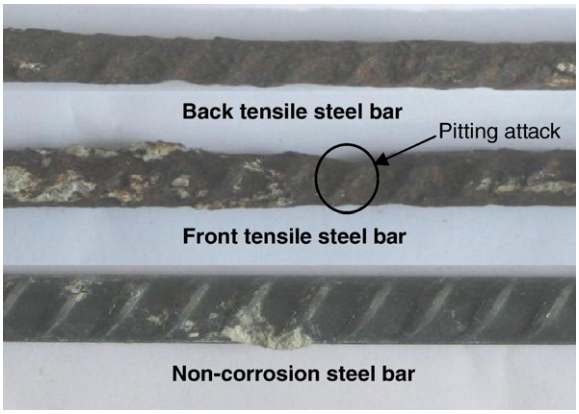

Fig. 9. Corrosion of the tensile steel bars in the central zone of B2CL1 after 23 years.

5. Discussion

5.1. Factors influencing corrosion pattern

Chloride-induced corrosion of steel in concrete is an electrochemical process. Even though the corrosion cells have been used to analyze reinforced concrete corrosion by many researchers, no general consensus has been reached for the definition of microcells and macrocells [11]. Microcells and macrocells are defined according to the different spatial locations of the anode and the cathode [12,13]. Anodes and cathodes for microcells corrosion are adjacent and more or less uniformly distributed along the reinforcement surface as shown in Fig. 15(a), resulting to a more or less uniform corrosion. On the contrary, for macrocells corrosion, anodic area is localized, inducing localized pitting attacks (Fig. 15(b)). But, both macrocells and microcells can occur simultaneously at the same location (Fig. 15(b)).

According to the experimental results obtained on beams B1CL1 and B2CL1, the corrosion patterns observed are different versus time, mechanical effects, bar location and corrosion crack width.

5.1.1. Transversal bending cracks

At the early beginning of the corrosion process, transversal bending cracks led to macrocells corrosion, the steel at the cracks tip acting as the anodic surface. As bending cracks always occur in front of the stirrups, this early macrocells corrosion affects mainly the stirrups. But after few months, a healing process of the bending cracks leads this macrocells corrosion to stop. Crack healing is due to the rust expansion entering and filling the gaps of cracks and to the re-hydration of cement. Then, according to the experimental ageing conditions of the study, bending cracks do not play a significant role on the long term corrosion process. More detailed information and discussion about the long term influence of bending cracks are available in [14,15]. Finally, the effect of the sustained loading on corrosion process concerns the parts of tensile concrete located between the bending cracks. This aspect is discussed further in section Mechanical damage.

5.1.2. "Top-bar" effect—steel bar location and orientation

Horizontal steel bars located in the upper part of concrete members are affected by the "top-bar" effect. The "top-bar" effect leads to voids formation under the reinforcing bars in regard to concrete casting direction [16,17]. These voids are located in regard to the bottom half part of the steel surface and are distributed almost all along the reinforcement. It is the case of B1CL1 and B2CL1 compressive steel bars. The voids lead to the formation of corrosion cells due to a different potential between the bonded upper half surface acting as the cathode and the lower half surface, with interface defects, acting as the anode [18,19]. In addition, on the lower half surface with interface defects microcells corrosion develops (Fig. 15(a)) leading a generalized corrosion (Fig. 16). This is why there is no preferential area for corrosion propagation along the bars in the compressive zone of the corroded beams. As shown in Fig. 16, no significant corrosion occurs on the upper

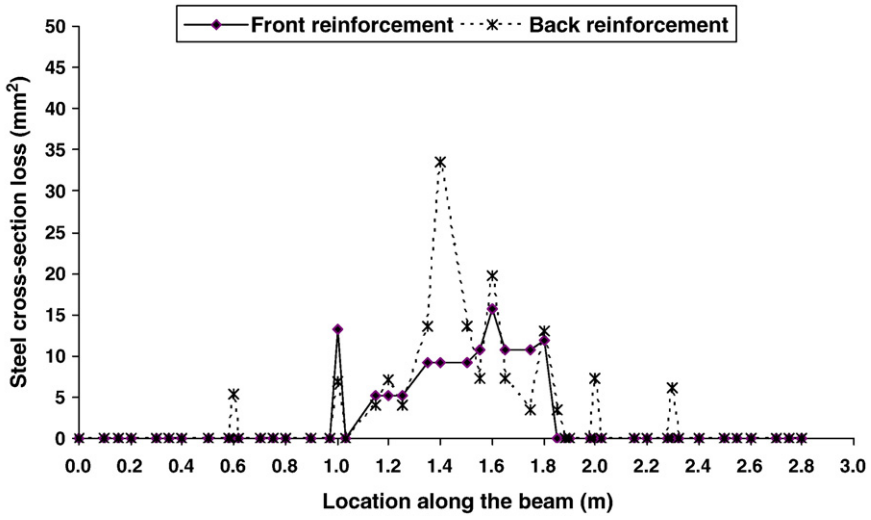

Fig. 10. Cross-section loss distribution along the tensile re-bars of B1CL1 after 14 years.

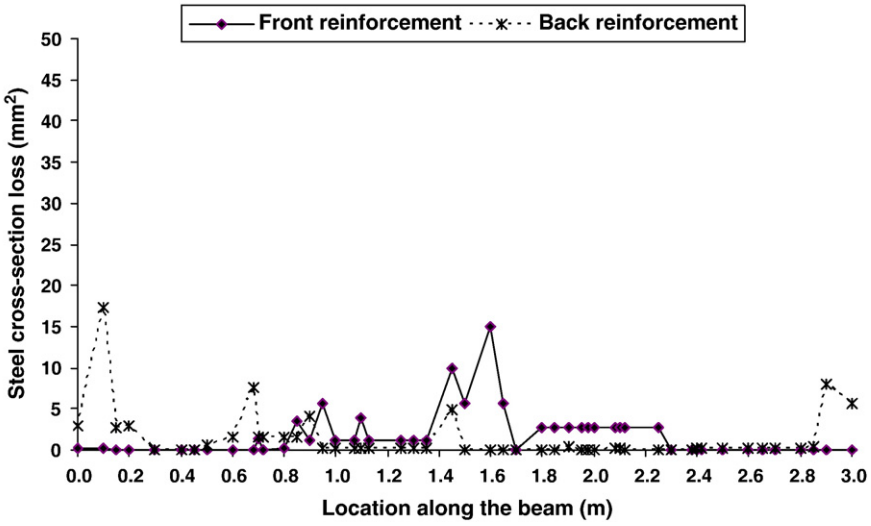

Fig. 11. Cross-section loss distribution along the compressive re-bars of B1CL1 after 14 years.

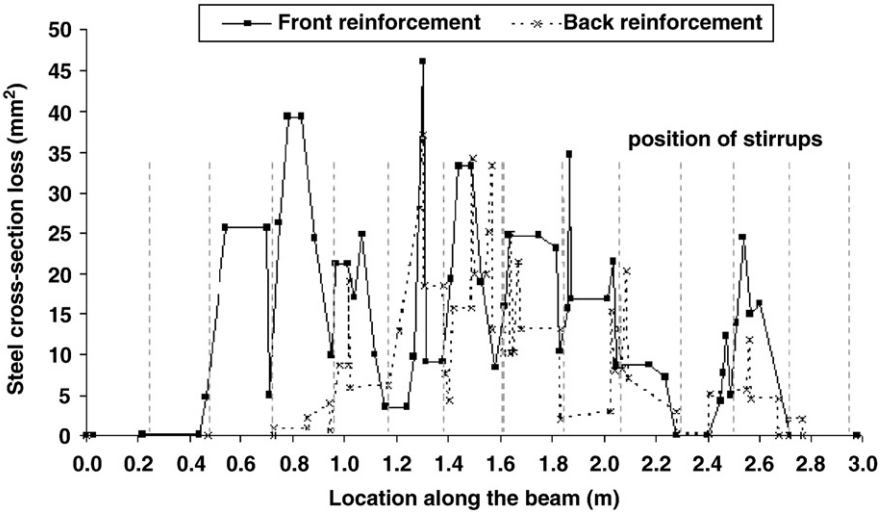

Fig. 12. Cross-section loss distribution along the tensile re-bars of B2CL1 after 23 years.

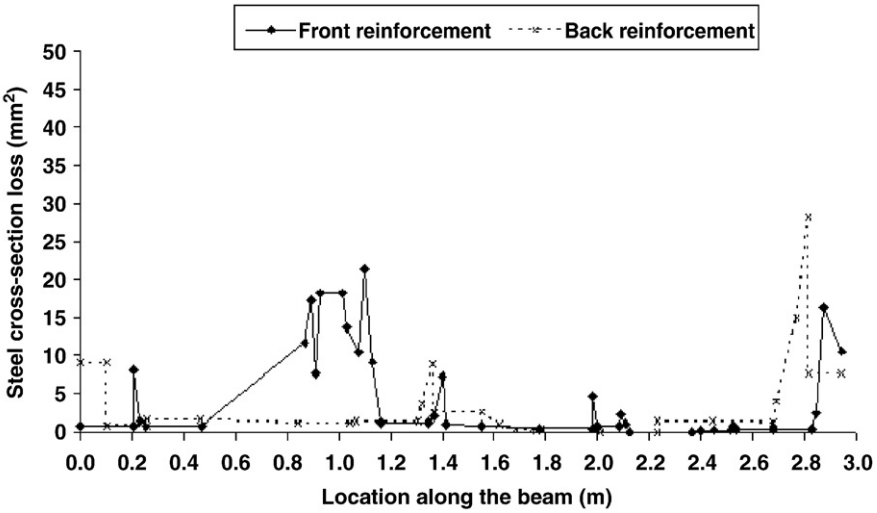

Fig. 13. Cross-section loss distribution along the compressive re-bars of B2CL1 after 23 years.

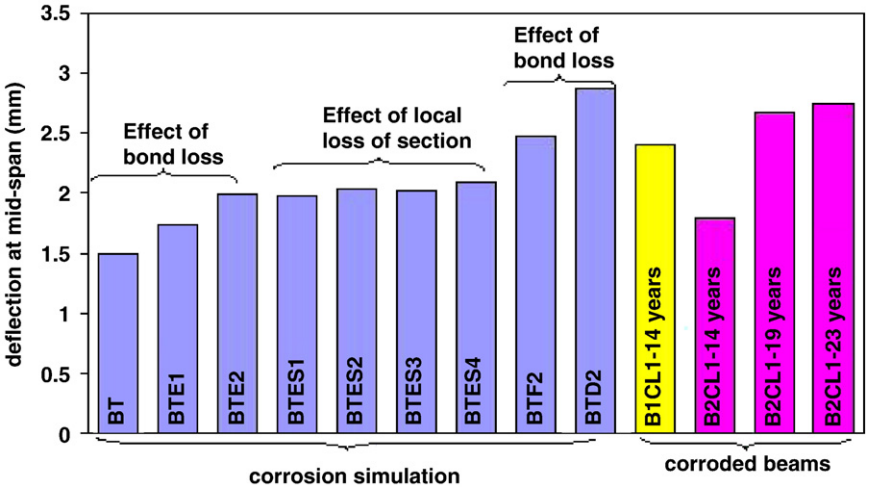

Fig. 14. Deflections measured on the corroded beams and obtained for the 9 steps of the corrosion simulation performed on BT control beam.

half part of the compressive bar (cathodic area) in spite of a huge chloride content at the steel depth reaching more than 2% of cement mass [8].

5.1.3. Mechanical damage

Corrosion of tensile re-bars was more concentrated in the central zone of the beams where the bending moment is maximum (Figs. 10 and 12). This is attributed to the influence of the sustained loading during the corrosion process. The sustained loading induces an increase in aggressive agent penetration within the concrete located between the bending cracks and a damage of the concrete–steel interface between the bending cracks [9,20]. The localized steel–concrete interface mechanical defects act as anodic surfaces and lead to macrocells corrosion (pitting attacks in Fig. 8(b)). Fig. 8(b) shows that the pitting attacks are mostly far from the stirrups location which corresponds to bending cracks location. This result shows that there is no direct correlation between the location of the bending cracks and long term pitting attacks propagation. As soon as the chloride

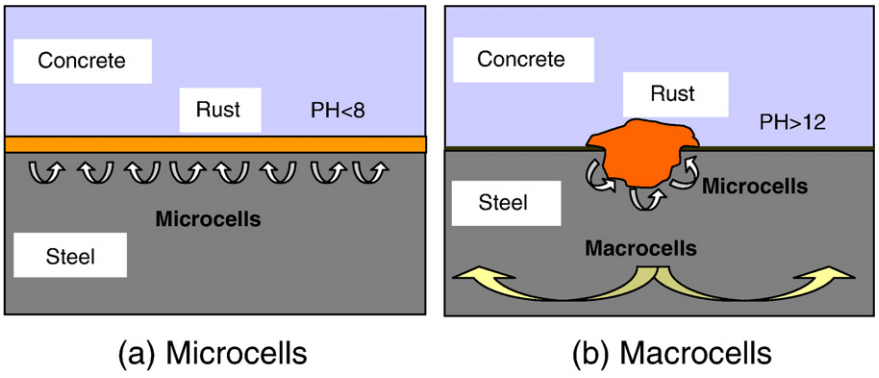

Fig. 15. Schematic representation of the corrosion cells of steel in concrete [13].

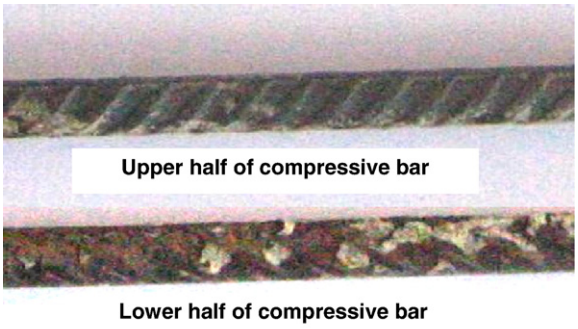

Fig. 16. Corrosion of the compressive rebar of B2CL1 due to the "top-bar" effect.

concentration exceeds the threshold values [21,22], corrosion propagates with a high rate due to the high ratio cathodic surface/anodic surface.

5.1.4. Corrosion longitudinal cracking

Versus time and corrosion longitudinal cracking development, the corrosion pattern is significantly modified. For small corrosion crack widths, localized pitting corrosion (macrocells corrosion) is the main corrosion pattern. Then, for wide crack width, generalized corrosion becomes the predominant corrosion pattern. Indeed, in addition to the better access for chloride and oxygen to the steel, the cracks interconnection and widening is equivalent to steel–concrete interface defects leading to a microcells corrosion as in the case of the bars affected by the "top-bar" effect (Fig. 15(a)). Fig. 17 shows that corrosion propagates only on the steel surface located in front of the crack along B2CL1 tensile bars where the cracks width were relatively low (about 1 mm for Fig. 17).

The critical crack width, which leads to the change in corrosion pattern, has not yet been clearly quantified. However, according to the experimental results, it should be a range between 0.5 mm and 1.5 mm. More works will be carried out in the L.M.D.C. to clarify this point.

5.2. Influence of corrosion on serviceability

The reinforcement corrosion leads to the reduction of the steel cross-section and the steel–concrete bond. The corrosion simulation performed in this study shows that the bond loss, in areas where the bending moment is maximum, is the main factor affecting the serviceability. Localized cross-section losses, up to 30% of initial area, do not influence the serviceability as the resulting increase in steel strain is too local to affect the mid-span deflection.

Consequently, under the localized corrosion pattern (early cracking stage), only the bond deterioration due to the local pitting corrosion should be taken into account in the analysis of the serviceability. Of course, the localized steel cross-section losses must be considered for ultimate capacity assessment [10,23].

Then, when corrosion is generalized (late cracking stage), as the steel–concrete bond is already lost, the generalized steel cross-section reduction becomes the main factor affecting the beams serviceability. But, at this stage, the deflection increase is slower due to the low general corrosion rate. Indeed, beam B2CL1 deflection did not increase a lot between 19 years and 23 years in spite of significant increase in cracks width (Figs. 6, 7 and 14).

6. Conclusion

- Corrosion of tensile steel bars:
  - In the corrosion cracking initiation period, localized corrosion due to macrocells corrosion firstly appears in areas where the bending moment is maximum. Localized pitting attacks are clearly observed, mostly located far from the bending cracks. These pitting attacks are attributed to localized steel–concrete interface mechanical defects.
  - At the early stage of corrosion cracks propagation, when crack width is inferior to a critical value ranging between 0.5 mm and 1.5 mm, macrocells corrosion is still the predominant pattern.
  - At late corrosion cracking stage, when the corrosion cracks interconnect and widths becomes superior to 1.5 mm, microcells corrosion leading to a generalized corrosion rapidly develops and becomes the predominant pattern.
- Effect of tensile steel corrosion on beams serviceability:
  - Under the localized pitting corrosion pattern, the serviceability is affected by the steel–concrete bond loss but not by the local steel cross-section reduction. The stiffness reduces a lot during corrosion cracking initiation and during the early period of cracks propagation (crack width up to about 1 to 1.5 mm).
  - When corrosion is generalized (late cracking stage), as the steel–concrete bond is already lost, the generalized steel cross-section reduction becomes the main factor affecting the beams serviceability. But, at this stage, the deflection increase is slower due to the low general corrosion rate.
- Corrosion of steel bars located in compressive zone:
  - The voids under the horizontal re-bars occurring due to the "top-bar effect lead to the formation of corrosion cells due to a different potential between the bonded upper half surface acting as the cathode and the lower half surface, with interface defects, acting as the anode. Simultaneously, microcells corrosion develops at the lower interface with interfacial defects leading to a generalized corrosion. Bonded upper half surface of the bar (cathodic surface) is not affected by the corrosion in spite of very high chloride contents.

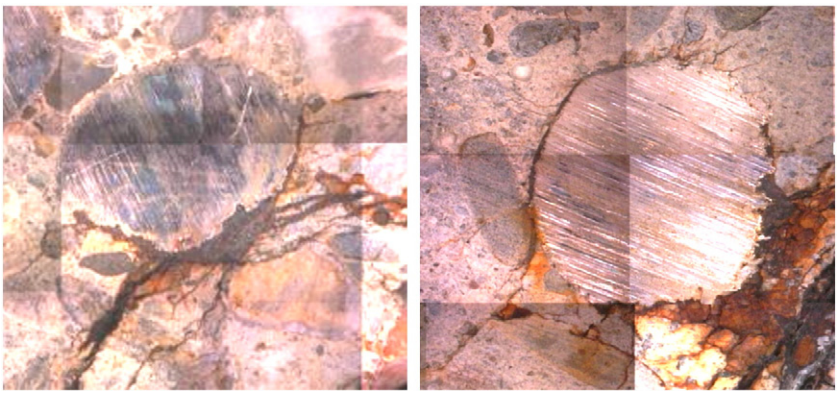

Fig. 17. Corrosion at the steel–concrete interface of tensile reinforcements (B2CL1).

References

[1] C. Andrade, C. Alonso, D. Garcfa, J. Rodriguez, Remaining lifetime of reinforced concrete structures: effect of corrosion on the mechanical properties of steel, International Conference on Life Prediction of Corrodible Structures, 1991, pp. 12/1–12/11, Cambridge, UK.

[2] C. Andrade, C. Alondso, F.J. Molina, Cover cracking as a function of bar corrosion: Part 1. Experimental test, Material and Structures 26 (1993) 453–464.

[3] J. Rodriguez, L.M. Ortega, J. Casal, Corrosion of reinforcing bars and service life of reinforced concrete structures: corrosion and bond deterioration, International Conference on Concrete across borders, Odense, Denmark, 1994, Vol.2, pp.315–326.

[4] J. Rodriguez, L.M. Ortega, J. Casal, Load carrying capacity of concrete structures with corroded reinforcement, Construction and Building Material 11 (4) (1997) 239–248.

[5] X. Fu, D.D.L. Chung, Effect of corrosion on the bond between concrete and steel rebar, Cement and Concrete Research 27 (12) (1997) 1811–1815.

[6] L. Amleh, S. Mirza, Corrosion influence on bond between steel and concrete, ACI Struct J 96 (3) (1999) 415–423.

[7] F. Paradis, V. Lapointe, M. Jolin, J. Marchand, Accelerated test methods to investigate chloride-induced steel corrosion damage in reinforced concrete—a brief review, in: V.M. Malhotra (Ed.), Seventh CANMET/ACI International Conference on Durability of Concrete, 2006, pp. 357–373, May 28–June 3, Montreal.

[8] T. Vidal, A. Castel, R. Francois, Corrosion process and structural performance of a 17 year old reinforced concrete beam stored in chloride environment, Cement and Concrete Research 37 (2007) 1551–1561.

[9] A. Castel, T. Vidal, R. François, G. Arliguie, Influence of steel–concrete interface quality on reinforcement corrosion induced by chlorides, Magazine of Concrete Research 55 (2) (April 2003) 151–160.

[10] A. Castel, R. François, G. Arliguie, Mechanical behavior of corroded reinforced concrete beams—Part 1: Experimental study of corroded beams, Materials and Structures 33 (Nov 2000) 539–544.

[11] P. Rodriguez, E. Ramirez, S. Feliu, J.A. Gonzalez, W. López, Significance of coplanar macrocells to corrosion of concrete–embedded steel, Corrosion 55 (3) (1999) 319–325.

[12] B. Elsener, Macrocell corrosion of steel in concrete—implications for corrosion monitoring, Cement & Concrete Composites 24 (2002) 65–72.

[13] M. Raupach, Chloride-induced macrocell corrosion of steel in concrete—theoretical background and practical consequences, Construction and Building Materials 10 (5) (1996) 329–338.

[14] R. François, G. Arliguie, J.C. Maso, Durabilite du beton arme soumis a l'action des chlorure, Annales de l'ITBTP 529 (1994) 1–48.

[15] R. François, G. Arliguie, Influence of service cracking on reinforcement steel corrosion, Journal of Materials in Civil Engineering 10 (1) (1998).

[16] P.R. Jeanty, D. Mitchell, M.S. Mirza, Investigation of top bar effects in beams, ACI Structural Journal 85 (3) (May–June. 1988) 251–257.

[17] T.A. Soylev, R. Francois, Corrosion of reinforcement in relation to presence of defects at the interface between steel and concrete 17 (4) (2005).

[18] T.U. Mohammed, H. Hamada, Corrosion of horizontal bars in concrete and method to delay early corrosion, ACI Materials Journal 103 (5) (September–October 2006).

[19] T.U. Mohammed, N. Otsuki, H. Hamada, Corrosion of steel bars in cracked concrete under marine environment, Journal of Materials in Civil Engineering, (ASCE) 0899-1561 15 (5) (2003) 460–469.

[20] A. Castel, O. Francy, R. François, G. Arliguie, Chloride diffusion in reinforced concrete beam under sustained loading, CANMET/ACI Fifth International Conference on Recent Advances in Concrete Technology, ACI SP 200, Singapore, July 29–August 1 2001, pp. 647–662, Farmington Hills, Michigan.

[21] ACI committee 222, Corrosion of metal in concrete, Journal Proceedings 82 (1) (1985) 3–32.

[22] RILEM technical committee 124-SRC, Draft recommendation for repair strategies for concrete structures damaged by reinforcement corrosion, Materials and Structures 27 (1994) 415–436.

[23] A. Castel, R. François, G. Arliguie, Mechanical behavior of corroded reinforced concrete beams—Part 2: Bond and notch effects, Materials and Structures 33 (Nov 2000) 545–551.